COMPUTATIONAL MICRO-MECHANICAL MODEL OF FLEXIBLE WOVEN FABRIC FOR FINITE ELEMENT IMPACT SIMULATION

Ala Tabiei[*] and Ivelin Ivanov[†]
The Center of Excellence in DYNA3D Analysis
Department of Aerospace Engineering and Engineering Mechanics
University of Cincinnati, OH 45221-0070, USA

ABSTRACT

This work presents a computational material model of flexible woven fabric for finite element impact analysis and simulation. The model is implemented in the nonlinear dynamic explicit finite element code LSDYNA. The material model derivation utilizes the micro-mechanical approach and the homogenization technique usually used in composite material models. The model accounts for reorientation of the yarns and the fabric architecture. The behavior of the flexible fabric material is achieved by discounting the shear moduli of the material in free state, which allows the simulation of the trellis mechanism before packing the yarns. The material model is implemented into the LSDYNA code as a user defined material subroutine. The developed model and its implementation is validated using an experimental ballistic test on Kevlar® woven fabric. The presented validation shows good agreement between the simulation utilizing the present material model and the experiment.

Keywords: computational material model, flexible woven fabric, textile composites, and explicit finite element ballistic impact simulation.

INTRODUCTION

The high modulus fibers such as Kevlar, Spectra, Aramid, Nylon, etc. are vastly used not only in composite materials, but also in netted fabric as structural element which has high strength and flexibility. These two properties are very important for impacted structures, since they allow the structure to withstand large transverse deflection and to absorb the high impact energy. Woven fabrics can be used in structures subjected to transverse loading like human body armors subjected to projectile impact. Another application of the high modulus flexible fabrics is the protective jackets in airplane jet engines. These jackets are placed around the jet engines in order to contain any broken blades from penetrating the engine casing and consequently the fuselage.

Modeling of the flexible fabric behavior under membrane and transverse loading is a challenging task. The difficulty comes from the dual behavior of the fabric. In the free state, the fabric material behavior resembles trellis mechanism [1] with big reorientation of the yarns.

---

[*] Assistant Professor and Director, author to whom correspondence should be addressed
[†] Graduate Research Assistant

Initially, fill and warp yarns are mutually perpendicular (Fig 1,a). The load is carried by the yarns in their axial direction only. In any other in-plane direction they are free to rotate up to some locking angle (Fig. 1,b). The fabric slightly resists shear strain (and yarn rotation) due to the friction between yarns. When the rotated yarns have reached the locking angle between yarns (Fig. 1,c), the area density of the fabric is the highest and the yarns are packed in a block that has anisotropic properties. Moreover, the properties of the packed fabrics are of a general anisotropic material with many inclined principle axes.

Some models of the flexible fabric material available in the literature use the pin-joined mechanism of bars. Ting et al. [2] and Shim et al. [3] modeled the fabric material as an orthogonal grid of pin-joined member elements. Contact algorithm and transverse pressure loading are the difficult problems in such models. The finite element mesh has to be in scale of the fabric structure, which presents some difficulties in the general use of such models. The friction and the locking angle constraints are absent in most of these models. Even if they have been introduced in such models, the behavior of the model after locking will not be adequate because of the lack of transverse interaction of the members.

Vinson and Zukas [4] and Taylor and Vinson [5] modeled the fabric as conical isotropic shells for ballistic impact analysis. As a result of isotropic material assumption the models are not able to distinguish the membrane directions, and as a result the behavior of the material is the same in all directions, which is not confirmed by experimental results. Johnson et al. [6] tried to amend that by modeling the fabric by both pin-joined members and thin membrane shells. Bi-linear stress-strain relationship is assumed for bar elements in order to simulate the dual behavior of the fabric before and after the locking of the trellis mechanism. The shell elements provide the contact surface in this model.

The impact and ballistic problems can be simulated successfully by means of non-linear dynamic finite element codes. Such codes are heavily used in many industries as they provide a powerful tool and cost effective process for simulation-based designs. Based on previous developments of woven fabric composite computational models [7,8,9], it was anticipated that the homogenization technique used in micro-mechanical models gives good results with respect to the complex anisotropy modeling of the flexible fabric structures. A micro-mechanical model of the woven fabric can account for the crimping of the fibers. Shell elements are better structural elements for contact problems and transverse pressure loading in the finite element method. Therefore it was decided to develop a model of the flexible woven fabric material, that can simulate a trellis mechanism with reorientation of the yarns and their locking, based on micro-mechanics. The developed computational material model is implemented in the dynamic explicit nonlinear finite element code LSDYNA as a user defined material model that is compatible with membrane shell elements. The model was utilized to solve a ballistic impact problem of woven fabric material. In what follows, a description of the model and its implementation is presented.

THE COMPUTATIONAL MICRO-MECHANICAL MODEL

The Representative Volume Cell (RVC) approach is utilized in the micro-mechanical model development. The interlacing yarn pattern of the flexible weave fabric is depicted in Figure 1. As a result of the deformations, the fill and the warp yarns are no longer orthogonal although at the unloaded state, they could be orthogonal (the angle between fill and warp

direction is a user input parameter in the formulation). The RVC in this case is a rectangle in the plane of the fabric with diagonals in the fiber directions (Fig. 1,b) rather than a square with mid-sides in the fiber directions, which is usually used in other models [7,8,9].

The RVC structure is shown in Figure 2. The RVC is divided into four sub-cells, two anti-symmetric sub-cells containing the undulated fill-yarn and two other anti-symmetric sub-cells containing the warp yarn. The direction of the yarn in each sub-cell is determined by two angles – the braid angle, θ, and the undulation angle of the yarn, which is different for the fill and warp-yarns, β_f and β_w, respectively.

The starting point for the homogenization of the material properties is the determination of the yarn stiffness matrices. The material of the yarn is assumed to be transversely isotropic:

$$[C'] = [S']^{-1} = \begin{bmatrix} \dfrac{1}{E_1} & -\dfrac{\nu_{12}}{E_1} & -\dfrac{\nu_{12}}{E_1} & 0 & 0 & 0 \\[2mm] -\dfrac{\nu_{12}}{E_1} & \dfrac{1}{E_2} & -\dfrac{\nu_{23}}{E_2} & 0 & 0 & 0 \\[2mm] -\dfrac{\nu_{12}}{E_1} & -\dfrac{\nu_{23}}{E_2} & \dfrac{1}{E_2} & 0 & 0 & 0 \\[2mm] 0 & 0 & 0 & \dfrac{1}{\mu G_{12}} & 0 & 0 \\[2mm] 0 & 0 & 0 & 0 & \dfrac{1}{\mu G_{23}} & 0 \\[2mm] 0 & 0 & 0 & 0 & 0 & \dfrac{1}{\mu G_{12}} \end{bmatrix}^{-1} , \qquad (1)$$

where E_1, E_2, ν_{12}, ν_{23}, G_{12} and G_{23} are Young's moduli, Poisson's ratios, and the shear moduli of the yarn material, respectively. μ is a discount factor, which is function of the braid angle, θ, and has value between μ_0 and 1. Initially, in free stress state, the discount factor is a small value ($\mu_0 \ll 1$) and the material has very small resistance to shear deformation if any. In this way, the material behaves like a trellis mechanism with small resistance against the rotation of the yarns, corresponding to the friction between yarns. When the locking occurs, the fabric yarns are packed and they behave like elastic media. The discount factor is unity in this case and the fabric material resists to the shear with its real shear moduli. The contracted notation for strain and stress components adopted here is: 1≅11, 2≅22, 3≅33, 4≅12, 5≅23, 6≅31. The material directions of the yarn are depicted in Figure 3. We assume different stiffness matrices for fill and warp yarns in order to model unbalanced woven fabric. When the yarn stiffness matrix of each sub-cell is determined in the material coordinate system, it is transformed to RVC coordinate system.

The transformation of the sub-cell stiffness matrices from the material coordinate system to the RVC coordinate system is performed by the formula:

$$[C] = [T]^{\text{T}} [C'][T] , \qquad (2)$$

where $[C]$ is the stiffness matrix in RVC coordinate system, $[C']$ is the stiffness matrix in material coordinate system and $[T]$ is the transformation matrix. The transformation matrix $[T]$ contains components depending on directional cosines of the material axes with respect to RVC coordinate system [10]:

$$[T]=\left[\begin{array}{ccc|ccc} l_1^2 & m_1^2 & n_1^2 & l_1 m_1 & m_1 n_1 & n_1 l_1 \\ l_2^2 & m_2^2 & n_2^2 & l_2 m_2 & m_2 n_2 & n_2 l_2 \\ l_3^2 & m_3^2 & n_3^2 & l_3 m_3 & m_3 n_3 & n_3 l_3 \\ \hline 2l_1 l_2 & 2m_1 m_2 & 2n_1 n_2 & (l_1 m_2 + l_2 m_1) & (m_1 n_2 + m_2 n_1) & (n_1 l_2 + n_2 l_1) \\ 2l_2 l_3 & 2m_2 m_3 & 2n_2 n_3 & (l_2 m_3 + l_3 m_2) & (m_2 n_3 + m_3 n_2) & (n_2 l_3 + n_3 l_2) \\ 2l_3 l_1 & 2m_3 m_1 & 2n_3 n_1 & (l_3 m_1 + l_1 m_3) & (m_3 n_1 + m_1 n_3) & (n_3 l_1 + n_1 l_3) \end{array}\right] ,(3)$$

$$=\left[\begin{array}{cc} [T_1] & [T_2] \\ [T_3] & [T_4] \end{array}\right]$$

where

$$l_1 = \cos\beta\cos\theta \quad, \quad m_1 = \cos\beta\sin\theta \quad, \quad n_1 = \sin\beta \,,$$
$$l_2 = -\sin\theta \qquad , \quad m_2 = \cos\theta \qquad , \quad n_2 = 0 \qquad , \qquad (4)$$
$$l_3 = -\sin\beta\cos\theta \,, \quad m_3 = -\sin\beta\sin\theta \,, \quad n_3 = \cos\beta \,,$$

are the directional cosines of the material axes in RVC coordinate system.

After the transformation, the sub-cell stiffness matrices are in the form of the stiffness matrices for generally anisotropic materials. The anti-symmetry between both fill yarn sub-cells, as well as, between both warp yarn sub-cells makes the transformation easier, because only two transformation matrices are necessary to be calculated and only two transformations are necessary to be performed. One can easily prove that the stiffness matrix of "F"-sub-cell in RVC coordinate system, $[C^F]$, is related to "f"-sub-cell stiffness matrix components in RVC coordinate system, C_{ij}^f, by the following relation:

$$[C^F]=\left[\begin{array}{cccccc} C_{11}^f & C_{12}^f & C_{13}^f & C_{14}^f & -C_{15}^f & -C_{16}^f \\ & C_{22}^f & C_{23}^f & C_{24}^f & -C_{25}^f & -C_{26}^f \\ & & C_{33}^f & C_{34}^f & -C_{35}^f & -C_{36}^f \\ & & & C_{44}^f & -C_{45}^f & -C_{46}^f \\ & sym & & & C_{55}^f & C_{56}^f \\ & & & & & C_{66}^f \end{array}\right] . \qquad (5)$$

The "W"-sub-cell stiffness matrix can be obtained from the "w"-sub-cell stiffness matrix components by using a similar relation. The transformed sub-cell stiffness matrices are homogenized in order to obtain the effective stiffness matrix of the RVC.

Homogenization Procedure

Mixed boundary conditions, iso-strain and iso-stress assumptions are adopted here for the homogenization of the sub-cell materials in the RVC [11]. The strain and stress components of constituents are divided into two groups – three iso-strain components and three iso-stress components:

$$\{\varepsilon\}_k = \left\{ \{\varepsilon_n\}_k^{\text{T}} \quad \{\varepsilon_s\}_k^{\text{T}} \right\}_k^{\text{T}} , \tag{6}$$

$$\{\sigma\}_k = \left\{ \{\sigma_n\}_k^{\text{T}} \quad \{\sigma_s\}_k^{\text{T}} \right\}_k^{\text{T}} , \tag{7}$$

where n-subscript denotes iso-strain components, s-subscript denotes iso-stress components and $k = f, w, F, W$ denotes the sub-cell, according to the adopted notation for them. The stiffness matrix of each constituent is split into four 3×3 matrices:

$$[C]_k = \begin{bmatrix} [C_{nn}]_k & [C_{ns}]_k \\ [C_{sn}]_k & [C_{ss}]_k \end{bmatrix} , \tag{8}$$

where $[C_{nn}]_k$ and $[C_{ss}]_k$ are symmetrical and $[C_{sn}]_k = [C_{ns}]_k^{\text{T}}$. The constitutive equations for each sub-cell now can be written as follows:

$$\{\sigma_n\}_k = [C_{nn}]_k \{\varepsilon_n\}_k + [C_{ns}]_k \{\varepsilon_s\}_k , \tag{9}$$

$$\{\sigma_s\}_k = [C_{sn}]_k \{\varepsilon_n\}_k + [C_{ss}]_k \{\varepsilon_s\}_k , \tag{10}$$

The effective properties of the homogenized volume are assumed to be volumetric averages of the constituent properties. Because the strain and stress are the same at all points of each constituent volume, the effective strain, $\{\bar{\varepsilon}\}$, and the effective stress, $\{\bar{\sigma}\}$, vectors can be expressed by the rule of mixture:

$$\{\bar{\varepsilon}\} = \sum_k f_k \{\varepsilon\}_k , \tag{11}$$

$$\{\bar{\sigma}\} = \sum_k f_k \{\sigma\}_k , \tag{12}$$

where f_k is the volume fraction of the k-th constituent in the homogenized volume. The effective strain and stress vectors are related by the effective stiffness matrix, $[\bar{C}]$, which is the ultimate aim of this procedure:

$$\{\bar{\sigma}\} = [\bar{C}]\{\bar{\varepsilon}\} . \tag{13}$$

Partitioning the effective stiffness matrix into four matrices, the constitutive equations for the homogenized material can be written as follows:

$$\{\bar{\sigma}_n\} = [\bar{C}_{nn}]\{\bar{\varepsilon}_n\} + [\bar{C}_{ns}]\{\bar{\varepsilon}_s\} , \tag{14}$$

$$\{\bar{\sigma}_s\} = [\bar{C}_{sn}]\{\bar{\varepsilon}_n\} + [\bar{C}_{ss}]\{\bar{\varepsilon}_s\} , \tag{15}$$

where

$$[\bar{C}] = \begin{bmatrix} [\bar{C}_{nn}] & [\bar{C}_{ns}] \\ [\bar{C}_{sn}] & [\bar{C}_{ss}] \end{bmatrix} . \tag{16}$$

Applying the mixed boundary conditions on the constituents, we have the following:

$$\{\bar{\varepsilon}_n\} = \{\varepsilon_n\}_k , \tag{17}$$

$$\{\bar{\sigma}_s\} = \{\sigma_s\}_k \ , \tag{18}$$

The rule of the mixture ((11) and (12)), applied to the remaining parts of the strain and stress components, leads to the following:

$$\{\bar{\varepsilon}_s\} = \sum_k f_k \{\varepsilon_s\}_k \ , \tag{19}$$

$$\{\bar{\sigma}_n\} = \sum_k f_k \{\sigma_n\}_k \ . \tag{20}$$

Substituting (17) and (18) in (10) and solving it, one obtains the following:

$$\{\varepsilon_s\}_k = [C_{ss}]_k^{-1} \{\bar{\sigma}_s\} - [C_{ss}]_k^{-1} [C_{sn}]_k \{\bar{\varepsilon}_n\} \ . \tag{21}$$

Then substituting iso-strain components of strain in (9) and again using (17) and (18), we have:

$$\{\sigma_n\}_k = \left([C_{nn}]_k - [C_{ns}]_k [C_{ss}]_k^{-1} [C_{sn}]_k\right)\{\bar{\varepsilon}_n\} + [C_{ns}]_k [C_{ss}]_k^{-1} \{\bar{\sigma}_s\} \ . \tag{22}$$

Next, by substituting (22) in (20) and (21) in (19), we obtain:

$$[\bar{\sigma}_n] = [C_1^*]\{\bar{\varepsilon}_n\} + [C_2^*]\{\bar{\sigma}_s\} \ , \tag{23}$$

$$[\bar{\varepsilon}_s] = [C_3^*]\{\bar{\sigma}_s\} - [C_4^*]\{\bar{\varepsilon}_n\} \ , \tag{24}$$

where

$$[C_1^*] = \sum_k f_k \left([C_{nn}]_k - [C_{ns}]_k [C_{ss}]_k^{-1} [C_{sn}]_k\right) \ , \tag{25.1}$$

$$[C_2^*] = \sum_k f_k [C_{ns}]_k [C_{ss}]_k^{-1} \ , \tag{25.2}$$

$$[C_3^*] = \sum_k f_k [C_{ss}]_k^{-1} \ , \tag{25.3}$$

$$[C_4^*] = \sum_k f_k [C_{ss}]_k^{-1} [C_{sn}]_k \ , \tag{25.4}$$

Finally, the constitutive equations for homogenized volume are obtained by solving (24) for $\{\bar{\sigma}_s\}$ and substituting it in (23):

$$\{\bar{\sigma}_s\} = [C_3^*]^{-1}[C_4^*]\{\bar{\varepsilon}_n\} + [C_3^*]^{-1}\{\bar{\varepsilon}_s\} \ , \tag{26}$$

$$\{\bar{\sigma}_n\} = \left([C_1^*] + [C_2^*][C_3^*]^{-1}[C_4^*]\right)\{\bar{\varepsilon}_n\} + [C_2^*][C_3^*]^{-1}\{\bar{\varepsilon}_s\} \ , \tag{27}$$

The effective stiffness matrix of the homogenized volume can be expressed as follows:

$$[\bar{C}_{nn}] = [C_1^*] + [C_2^*][C_3^*]^{-1}[C_4^*] \ , \tag{28.1}$$

$$[\bar{C}_{ns}] = [C_2^*][C_3^*]^{-1} \ , \tag{28.2}$$

$$[\overline{C}_{sn}] = [C_3^*]^{-1}[C_4^*] = [\overline{C}_{ns}]^{\mathrm{T}} \ , \tag{28.3}$$

$$[\overline{C}_{ss}] = [C_3^*]^{-1} \ , \tag{28.4}$$

The RVC is discretized by the sub-cells. In order to provide continuity of the RVC in the membrane shell element plane, which is the proper FE for fabric modeling, in-plane iso-strain boundary conditions are applied for *xy*-plane of the RVC. The out-of-plane stress components of the sub-cells are equal to the RVC out-of-plane stress components. The imposed in-plane iso-strain and out-of-plane iso-stress boundary conditions can be written by means of the adopted contracted notation of components, as follows:

$$\varepsilon_1^f = \varepsilon_1^w = \varepsilon_1^F = \varepsilon_1^W \ , \quad \varepsilon_2^f = \varepsilon_2^w = \varepsilon_2^F = \varepsilon_2^W \ , \quad \varepsilon_4^f = \varepsilon_4^w = \varepsilon_4^F = \varepsilon_4^W \ ,$$
$$\sigma_3^f = \sigma_3^w = \sigma_3^F = \sigma_3^W \ , \quad \sigma_5^f = \sigma_5^w = \sigma_5^F = \sigma_5^W \ , \quad \sigma_6^f = \sigma_6^w = \sigma_6^F = \sigma_6^W \ , \tag{29}$$

where 1≅*xx*, 2≅*yy*, 3≅*zz*, 4≅*xy*, 5≅*yz*, 6≅*zx*, according to the notation of the RVC coordinate system.

The volume fractions of the constituents are equal for balanced fabric material, $f_f = f_w = f_F = f_W = 1/4$. In case of unbalanced fabric, proper volume fraction has to be calculated.

The calculated effective stiffness matrix represents the elastic properties of the fabric material. Because of the anti-symmetry of the sub-cells and the form of their stiffness matrices (5) in RVC coordinate system, the form of the effective stiffness matrix is as follows:

$$[\overline{C}] = \begin{bmatrix} \overline{C}_{11} & \overline{C}_{12} & \overline{C}_{13} & \overline{C}_{14} & 0 & 0 \\ \overline{C}_{12} & \overline{C}_{22} & \overline{C}_{23} & \overline{C}_{24} & 0 & 0 \\ \overline{C}_{13} & \overline{C}_{23} & \overline{C}_{33} & \overline{C}_{34} & 0 & 0 \\ \overline{C}_{14} & \overline{C}_{24} & \overline{C}_{34} & \overline{C}_{44} & 0 & 0 \\ 0 & 0 & 0 & 0 & \overline{C}_{55} & \overline{C}_{56} \\ 0 & 0 & 0 & 0 & \overline{C}_{56} & \overline{C}_{66} \end{bmatrix} . \tag{30}$$

Implementing the micro-mechanical model into a membrane shell element formulation, we can abandon the calculation of components $\overline{C}_{55}$, $\overline{C}_{56}$ and $\overline{C}_{66}$, because the corresponding stress and strain components are always zero. This makes the code more computationally efficient.

The instantaneous stiffness matrix is used to obtain the stress response of the fabric due to an increment of strain at each time step in the explicit finite element code. Note that the proposed material model is purposed for membrane shell elements and this is very important requirement for proper modeling of the fabric behavior. In tension, the FE model behavior is governed by the material model, while in compression, the FE model behavior is governed by the buckling phenomenon because of the lack of flexural stiffness in membrane elements. In this way, the micro-mechanical model and the membrane shell formulation are mutually complemented in order to represent truly the fabric behavior.

Fiber Reorientation

The proposed micro-mechanical model is developed to account for the reorientation of the yarns. At any time the micro-model corresponds to some current state of the deformed RVC, when the directions of the yarns are different from the initial ones. The reorientation of the yarns involves geometrical non-linearity. Therefore, a proper nonlinear method has to be used to solve for such a non-linearity. The utilized nonlinear method is the strain controlled incremental approach of the semi-discretization spatial approach employed in the explicit nonlinear finite element code.

The directions of the fill and the warp yarns in *xyz*-coordinate system are determined by the unit vectors $\{q_f\}$ and $\{q_w\}$, respectively. $\{q_f\}$ is the directional vector of fill yarn material axis 1 in "*f*"-sub-cell, while $\{q_w\}$ is the directional vector of warp yarn material axis 1 in "*w*"-sub-cell. In Figure 4., only the projection of the RVC in the *xy*-plane is given. Initially, the yarn directional unit vectors are calculated from the initial values of the angles θ, β_f, β_w:

$$\{q_f\} = \{\cos\beta_f \cos\theta \quad \cos\beta_f \sin\theta \quad \sin\beta_f\}^T , \tag{31}$$

$$\{q_w\} = \{\cos\beta_w \cos\theta \quad \cos\beta_w \sin\theta \quad \sin\beta_w\}^T . \tag{32}$$

The deformation gradient tensor, $[F]$ can be constructed from the engineering strain increment vector components:

$$[F]^T[F] = [I] + 2[E] = [U] = [Q]^T[D][Q] , \tag{33}$$

where $[I]$ is identity matrix, $[E]$ - the strain increment matrix, $[Q]$ – an orthogonal matrix, and $[D]$ is a diagonal matrix with eigenvalues of $[U]$ matrix. The singular value decomposition can be easily calculated, because the $[U]$ matrix for membrane shell elements has the form:

$$[U] = \begin{bmatrix} 1+2\Delta\varepsilon_1 & \Delta\varepsilon_4 & 0 \\ \Delta\varepsilon_4 & 1+2\Delta\varepsilon_2 & 0 \\ 0 & 0 & 1+2\Delta\varepsilon_3 \end{bmatrix} . \tag{34}$$

In this way, the deformation gradient could be found from singular value decomposition of $[U]$:

$$[F] = [Q]^T \sqrt{[D]} [Q] . \tag{35}$$

In the case of infinitesimal strains, we can determine the deformation gradient, in simpler way:

$$[F] = [I] + [E] = \begin{bmatrix} 1+\Delta\varepsilon_1 & \dfrac{\Delta\varepsilon_4}{2} & 0 \\ \dfrac{\Delta\varepsilon_4}{2} & 1+\Delta\varepsilon_2 & 0 \\ 0 & 0 & 1+\Delta\varepsilon_3 \end{bmatrix} . \tag{36}$$

Now, the yarn directional unit vectors are rotated to their new positions and normalized:

$$\{q_f'\} = [F]\{q_f\}, \quad \{q_w'\} = [F]\{q_w\} , \tag{37}$$

$$\{q_f\} = \{q_f'\}/\|\{q_f'\}\|, \quad \{q_w\} = \{q_w'\}/\|\{q_w'\}\| , \tag{38}$$

The new values of the angles determining the fiber directions are calculated from yarn directional unit vector components as follows:

$$\beta_f = \sin^{-1} q_{f3} , \quad \beta_w = \sin^{-1} q_{w3} , \tag{39}$$

$$\theta = \frac{\tan^{-1}(q_{f2}/q_{f1}) - \tan^{-1}(q_{w2}/q_{w1})}{2} , \tag{40}$$

The above-calculated angles can be used at each incremental step to calculate the instantaneous effective stiffness matrix of the RVC. These stiffness matrices consider the actual oriented yarns. When we use incremental approach for the non-linear finite element analysis, the strain increment is usually very small and satisfies the condition of infinitesimal strain, i.e. the strain increment to be very small compared to unity, therefore the expression (36) can be used. This is true for the explicit FE method, because of the inherent small time step used in the method.

The initial values of the yarn orientation angles can be given by the user. Usually, we assume that initially the fabric model is in a free state with braid angle equal to 45°. The undulation angle, in fact, is changing along the yarn and it varies from zero to some maximal value less than 90°. The maximal value of the undulation angle is usually used as characteristic of the crimping. For the proposed model, the undulation angle is an average value characterizing the material principle directions of the sub-cell. The angle which tangent is the half of the fabric thickness divided by the distance between the yarns can be considered as a good approximation of the undulation angle needed for the micro-mechanical model.

The discount factor, μ, is a function of the braid angle and it has to switch the model from trellis mechanism to elastic media and vise versa. In order to avoid high frequency oscillations due to the sudden stiffness change, a piece-wise function with a linear part in the transition range is chosen for the discount factor as follows:

$$\mu = \begin{cases} 1, & \theta < \theta_{dn} - \Delta\theta \\ \mu_0 + (1-\mu_0)(\theta_{dn} - \theta)/\Delta\theta, & \theta \in [\theta_{dn} - \Delta\theta, \theta_{dn}] \\ \mu_0, & \theta \in (\theta_{dn}, \theta_{up}) \\ \mu_0 + (1-\mu_0)(\theta - \theta_{up})/\Delta\theta, & \theta \in [\theta_{up}, \theta_{up} + \Delta\theta] \\ 1, & \theta > \theta_{up} + \Delta\theta \end{cases} \tag{41}$$

where $\theta_{dn} = 45° - \theta_{lock}$ is the lowest locking angle, $\theta_{up} = 45° + \theta_{lock}$ is the highest locking angle, θ_{lock} is the range to the locking angles (Figure 4.), and $\Delta\theta$ is the transition range of the braid angle. The graph of the above function is given in Figure 5.

The range to the locking angle, θ_{lock} , can be obtained from the yarn width and the spacing parameter of the fabric using simple geometrical relationship [1]. The transition range, $\Delta\theta$, can be chosen to be as small as possible, but big enough to prevent high frequency oscillations in transition to compacted state and depends on the range to the locking angle and the dynamics of the simulated problem. The minimal discount factor, μ_0, should provide very small shear resistance and negligible tension in the yarns when the tension in bias direction is applied and the yarns are still opened. The best way, of course, these parameters to be chosen is if we have force-displacement curve recorded during the trellis frame tension test of the fabric in

bias direction of loading [1]. Then we can choose the parameters to simulate and fit the force-displacement curve to the recorded one in the experiment.

NUMERICAL RESULTS

The developed woven flexible fabric material model is programmed as a user defined material subroutine in the LSDYNA finite element software. The implementation in LSDYNA is for balanced woven fabrics. The user defined material model works with reduced and fully integrated membrane shell elements. The capability of the model to simulate the behavior of fabric structures in dynamic problems was examined with simulating a ballistic impact problem. The results of the simulation are compared to the experimental result described in [12].

Ballistic impact of a blunt projectile onto Kevlar® 129 piece of fabric was simulated. The projectile has mass 2.8 g and initial velocity 341 m/s. The projectile is a cylinder with diameter and height of 5.38 mm. The elastic properties of the fabric material are:

$$E_1 = 99.1\,GPa \quad, \quad E_2 = 7.4\,GPa, \quad G_{12} = 2.5\,GPa,$$
$$G_{23} = 5.0GPa, \quad \nu_{12} = 0.2 \quad\quad, \quad \nu_{23} = 0.2 \quad\quad .$$

The fabric architecture is $\beta_f = \beta_w = 1°$, $\theta_{lock} = 5°$, $\Delta\theta = 0.5°$ and the discount factor is $\mu_0 = 1 \times 10^{-5}$. The fabric model has dimensions of 200×200×4.75 mm and was meshed by quad membrane elements.

The results of the ballistic impact simulation can be seen in Fig. 6 as sequential images of deflected fabric surface and its profile. The shape of the deflected area is similar to quadratic pyramid, which is confirmed by the experiments [12]. The time history of the projectile displacement (Fig. 7) and the projectile velocity (Fig. 8) almost coincide with those in [12]. The history of the contact force between the projectile and the fabric is given in Fig. 9 and the fully absorbed kinetic energy history is given in Fig. 10. The different reorientation of the yarns in the finite elements depending on their position on the deflected surface is observed in the FE simulation. The difference is in the direction of the braid angle change. As it can be seen in Fig. 11. the yarns in some elements are being opened, while in the others, they are being closed. This demonstrates how the trellis mechanism simulation of the material model works in the ballistic impact FE simulation.

In order to demonstrate the behavior of the fabric model further, we simulated airbag inflation of a closed cylinder. The example is a cylinder with conical bottoms suspended on two springs. The orientation of the yarns is in ±45° with respect to the axial direction. The mass flow of the air in the airbag is ramp and the graph of this loading is shown in Fig. 1. The properties of the transversely isotropic yarn material are as follows:

$$E_1 = 200\ MPa, E_2 = 10\ MPa, G_{12} = G_{23} = 38\ MPa, \nu_{12} = \nu_{23} = 0.2 .$$

The angle range to the locking is 20° from the initial position of the yarns and it allows the fabric model to stay open during the simulation. The discount factor of the shear modulus is 1×10^{-4}. The closed thin cylinders under uniform internal pressure have 2D-stress with a ratio of the hoop stress to the axial stress equals 2:1. This difference drives the yarns of the loosely woven fabric material to get closer in the hoop direction and opener in the axial direction. As a result of the

deformation, the airbag shrinks in axial direction and swells in transverse direction. A demonstration of this behavior is depicted by successive states of the simulation in Fig. 2.

The axial length change of the airbag is shown in Fig. 3. We can read 34 mm shrinking, which can be considered as significant. The diameter change of the cylinder is shown in Fig. 4. The swelling of the airbag in the transverse direction is approximately 15 mm. The airbag volume change as a result of the dimension change is shown in Fig. 5. The volume change is proportional to the squared diameter change and to the axial length change. The volume change of the airbag influences the pressure in the airbag. The development of the pressure is shown in Fig. 6. This kind of behavior is mainly due to the change of the angle between yarns. The graph of the angle change is shown in Fig. 7. A mutual rotation of 18 degree can be read for the yarns.

Suppressing the shear modulus discount and the yarn reorientation tracking in the fabric model, we get a solid material model, which is suitable for tightened woven fabrics. The tightened woven fabrics have very different behavior. The behavior of the tightened woven fabric model is shown in Fig. 8 by the first and the last state of the simulation of inflated airbag. No visual change of the shape can be found. The axial length change is given in Fig. 9 and the diameter change is in Fig. 10. Both show insignificant swelling in all directions. The volume change is shown in Fig. 11 and the pressure change is in Fig. 12.

CONCLUSION

The developed micro-mechanical material model of flexible woven fabric can model the dual behavior corresponding to the real behavior of the fabric material. It can represent the trellis mechanism behavior before the locking of the yarns and the generally anisotropic elastic properties of the fabric material after packing of the yarns. The model can be successfully utilized to represent the behavior of flexible woven fabrics under transverse loading in FE simulation codes. The model shows very good capability for simulating ballistic impact problems and is validated through an experimental test.

ACKNOWLEDGMENT

REFERENCES

1. T.M. McBride, "The large deformation behavior of woven fabrics and microstructural evaluation in formed textile composites", *Ph. D. Dissertation, Boston University, College of Engineering*, (1997).

2. J. Ting, D. Roylance, C.H. Chi and B. Chitrangad, "Numerical modeling of fabric panel response to ballistic impact", *Proceedings of the 25th International SAMPE Technical Conference*, October 26-28, (1993).

3. V.P.W. Shim, V.B.C. Tan and T.E. Tay, "Modeling deformation and damage characteristics of woven fabric under small projectile impact", *International Journal of Impact Engineering*, **16**, 585-605, (1995).

4. J.R. Vinson and J.A. Zukas, "On the ballistic impact of textile armor", *Journal of Applied mechanics*, **6**, 263-268, (1975).

5. W.J. Jr. Taylor and J.R. Vinson, "Modeling ballistic impact into flexible materials", *AIAA Journal*, **28**, 2098-2103, (1990).

6. G.R. Johnson, S.R. Beissel, and P.M. Cunniff, "A computational model for fabric subjected to ballistic impact", *Proceedings of the 18th International symposium on ballistics, San Antonio, TX*, November 15-19, (1999).

7. A. Tabiei and Y. Jiang, "Woven fabric composite material model with material nonlinearity for nonlinear finite element simulation", *International Journal of Solids and Structures*, **36** (18), 2757-2771, (1999).

8. A. Tabiei, Y. Jiang, and Y. Witao, "Novel micromechanics-based woven fabric composite constitutive model with material nonlinear behavior", *AIAA Jounal*, **38** (8), 1437-1443, (2000).

9. R. Tanov and A. Tabiei, "Computationally Efficient Micromechanical Woven Fabric Composite Elastic Constitutive Models", *Journal of Applied Mechanic,* Vol 68, march 2001.

10. R.D. Cook, D.S. Malkus, and M.E. Plesha, "Concepts and applications of finite element analysis", New York: Wiley, 3rd edition, (1989).

11. M. Karayaka and P. Kurath, "Deformation and failure behavior of woven composite laminates", *Journal of Engineering Materials and Technology*, **116**, 222-232, (April 1994).

12. D. Starratt, G. Pageau, R. Vaziri, and A. Poursartip, "An instrumented experimental study of the ballistic impact response of Kevlar® fabric", *Proceedings of the 18th International symposium on ballistics, San Antonio, TX*, November 15-19, (1999).

a) Free state

Representative
Volume Cell

b) Stretched

c) Compacted
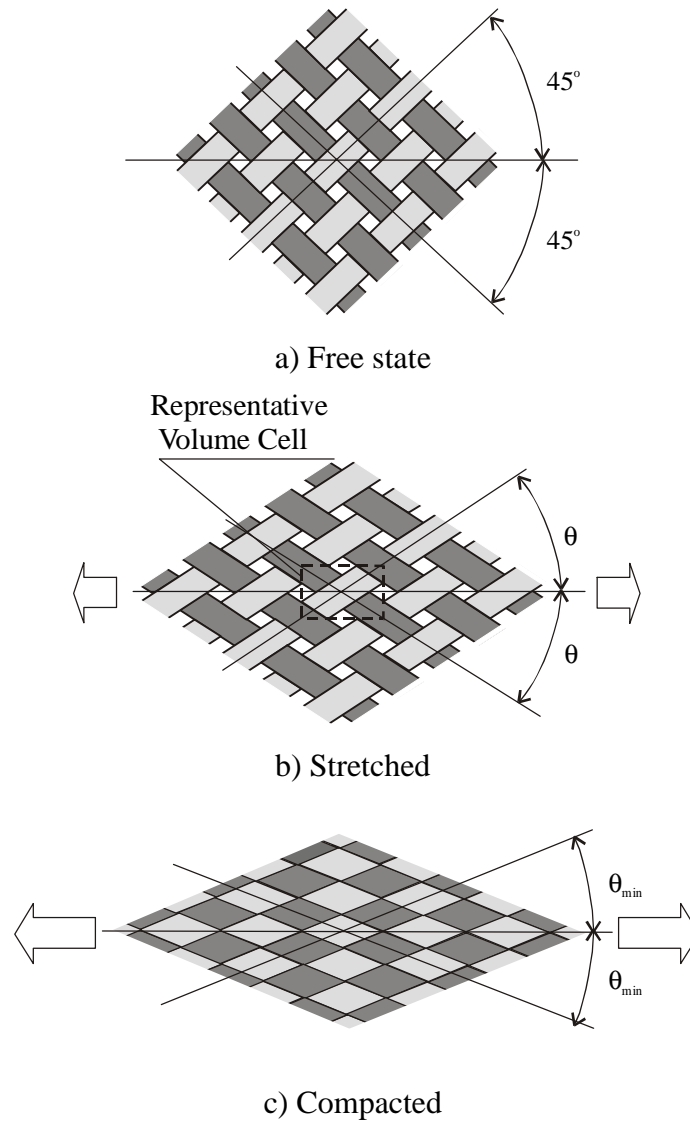
Fig. 1. Plain-woven fabric interlacing pattern.
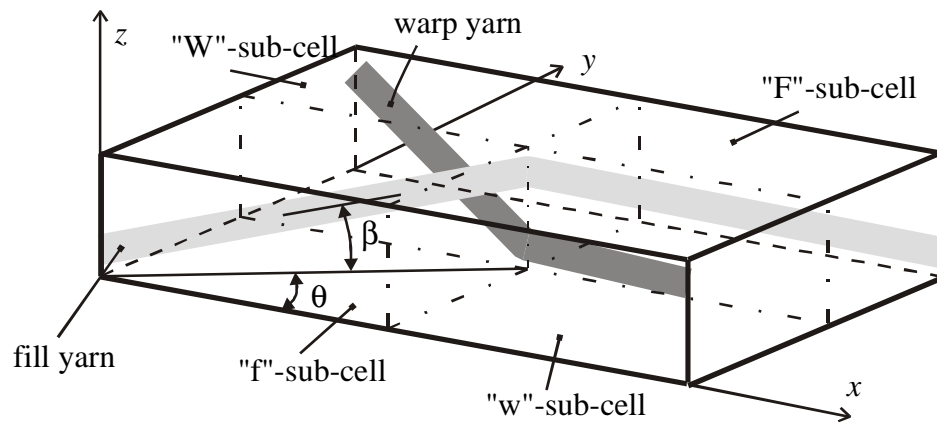
Fig. 2. Micro-mechanical model.
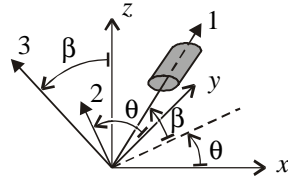
Fig. 3. Yarn orientation.
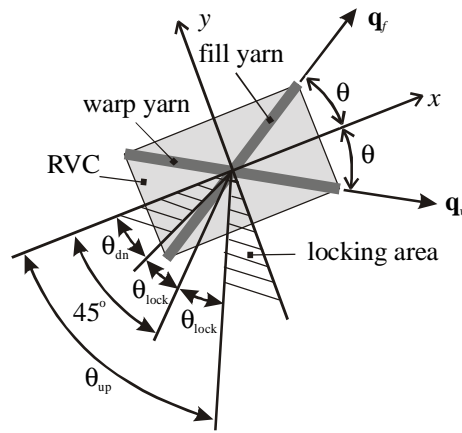
Fig. 4. Locking angles.
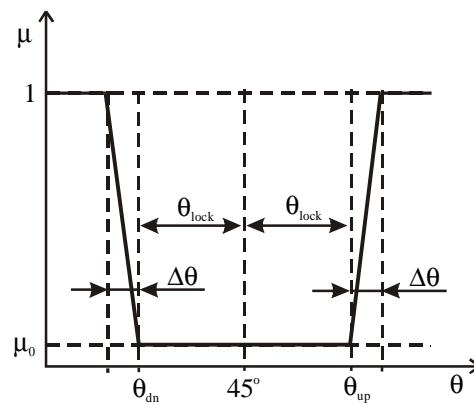
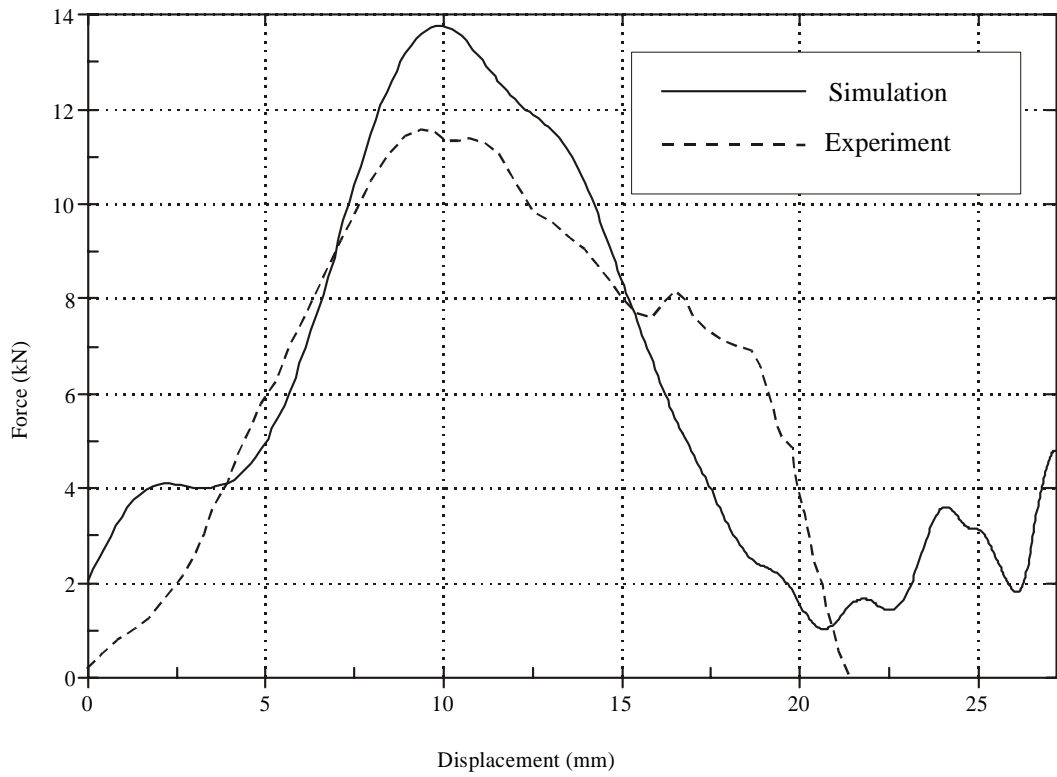***Fig. 5.*** Discount factor, μ, as a function of braid angle, θ.

Time = 3.4391e-05

Time = 3.4391e-05

Time = 7.0445e-05

Time = 7.0445e-05

Time = 0.00010494

Time = 0.00010494

Time = 0.00014087

Time = 0.00014087

Time = 0.00017542

Time = 0.00017542

Time = 0.0002114

Time = 0.0002114
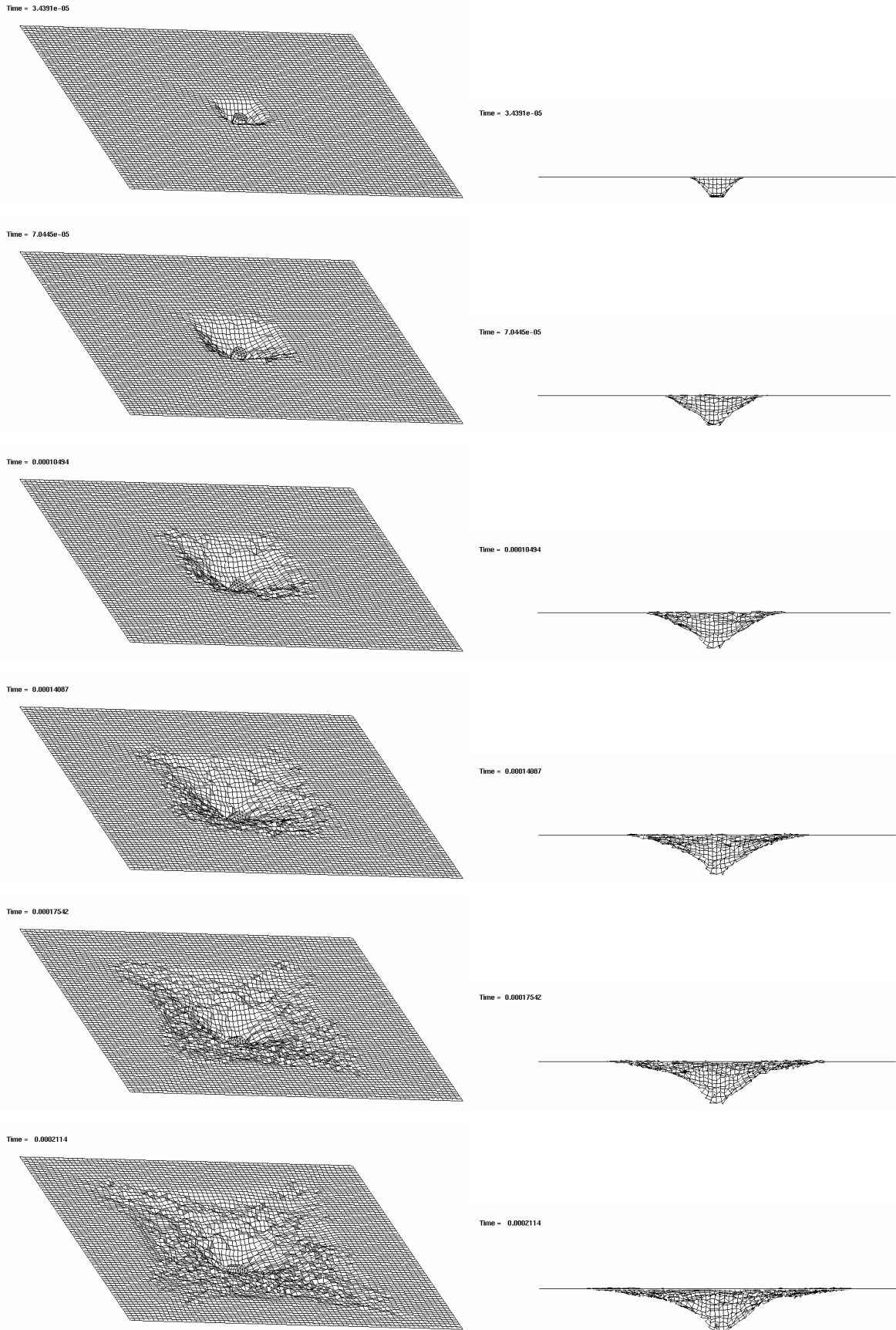
Fig. 6. Deflection of the fabric surface impacted by a projectile
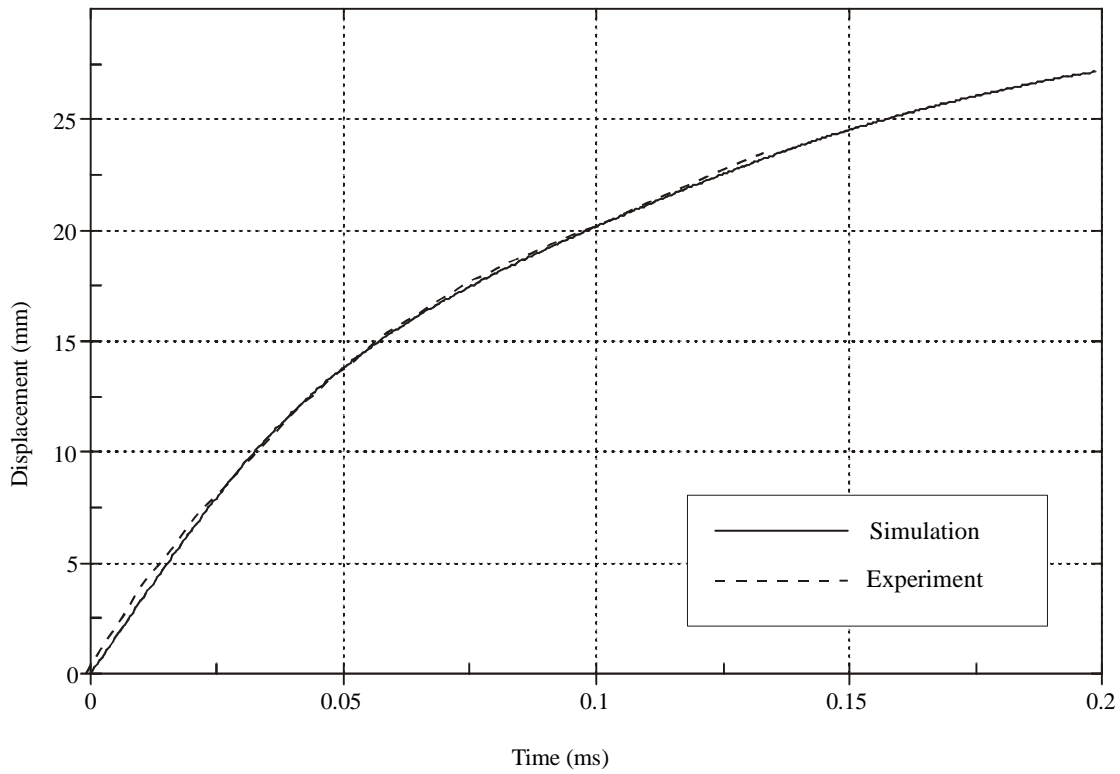
Fig. 7. Projectile displacement
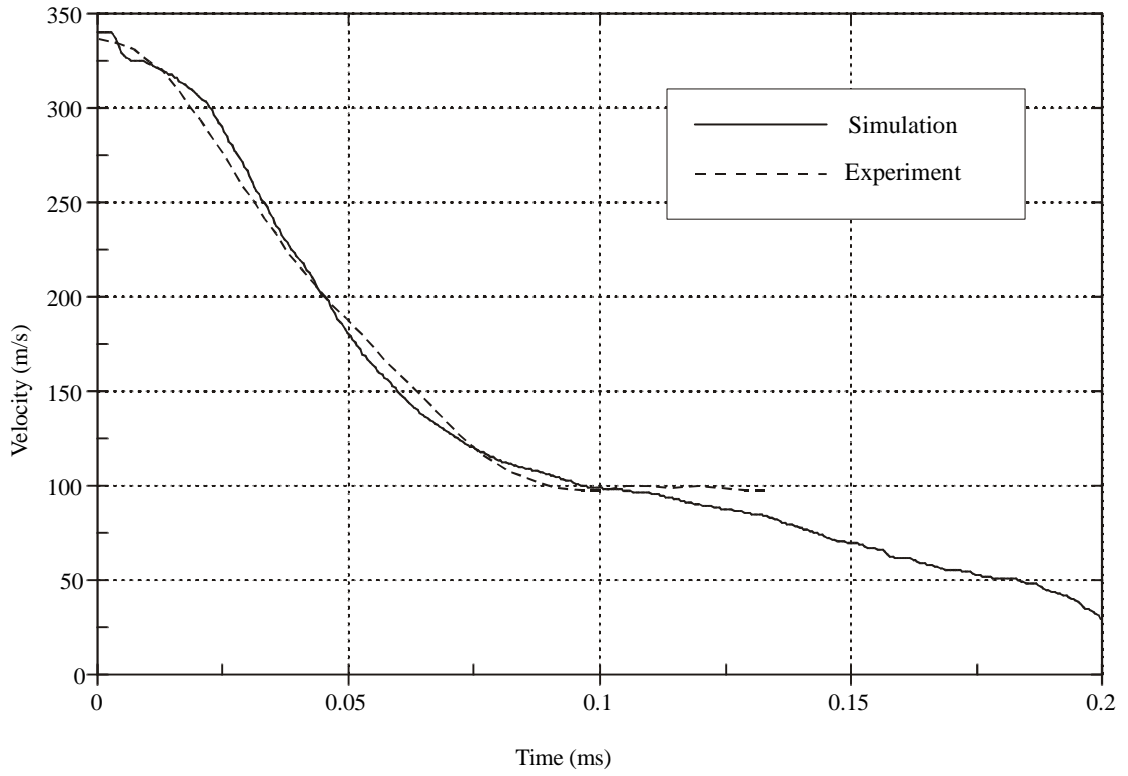
Fig. 8. Projectile velocity

Fig. 9. Contact force between the projectile and the fabric
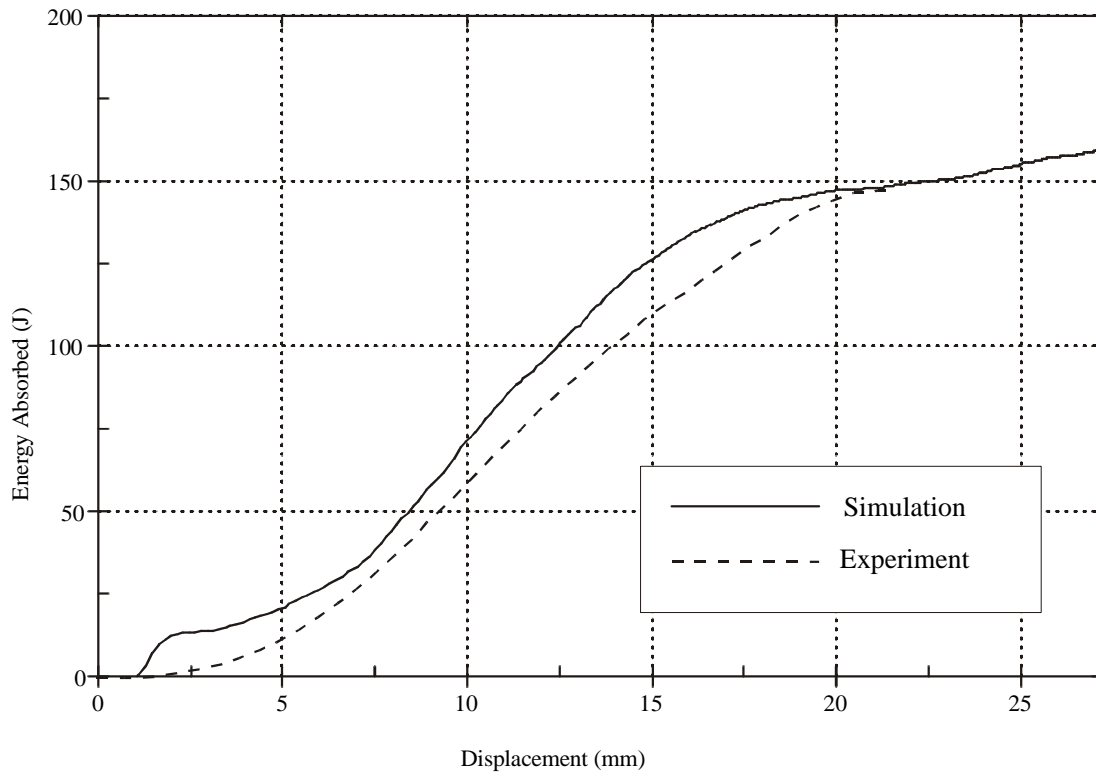
Fig. 10. Energy absorbed by the fabric.
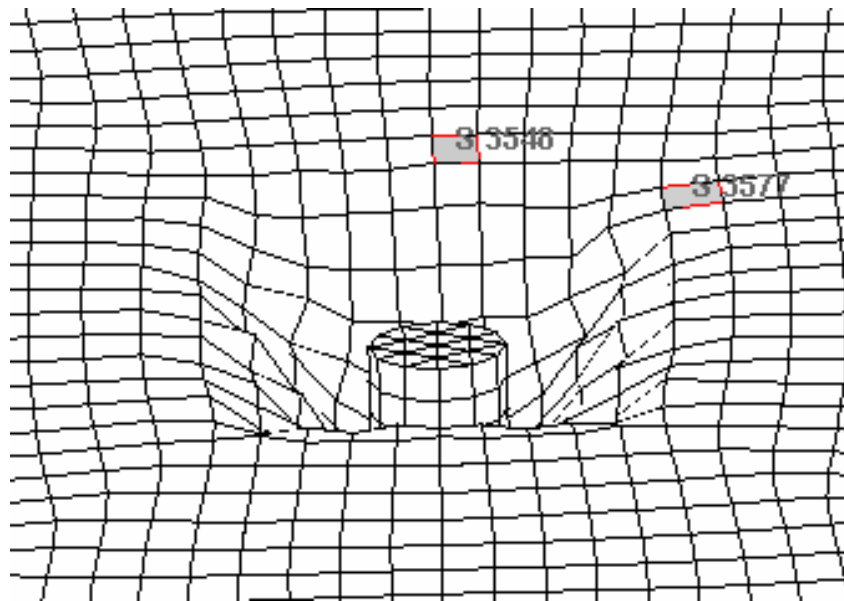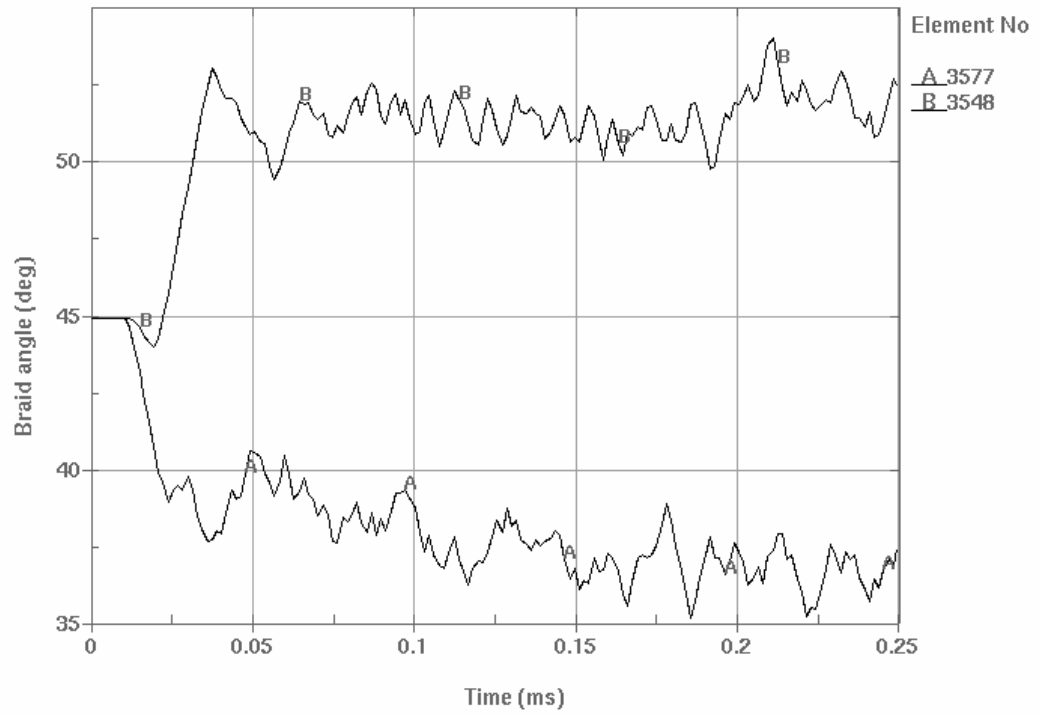
Fig. 11. Braid angle change of two different elements and their position on the surface of impacted fabric model.
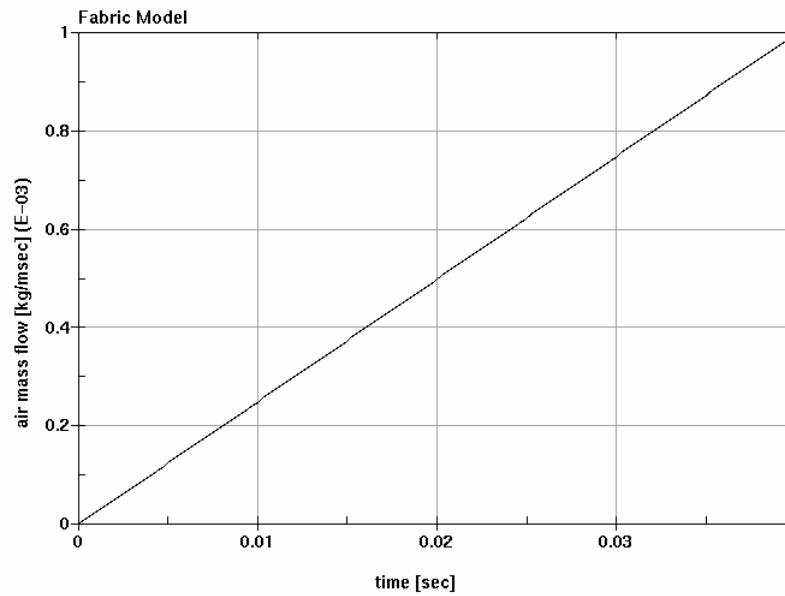
Fig. 1. Air mass flow as ramp loading.

Fabric Model – reorientation and shear modulus discount
Time = 0
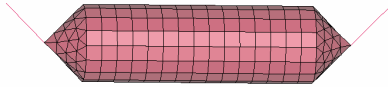
Fabric Model – reorientation and shear modulus discount
Time = 0.0094843

Fabric Model – reorientation and shear modulus discount
Time = 0.019491
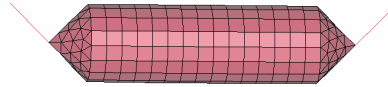
Fabric Model – reorientation and shear modulus discount
Time = 0.029986

Fabric Model – reorientation and shear modulus discount
Time = 0.040006

Fig. 2. Successive states of short airbag with loosely woven fabric model inflation simulation.
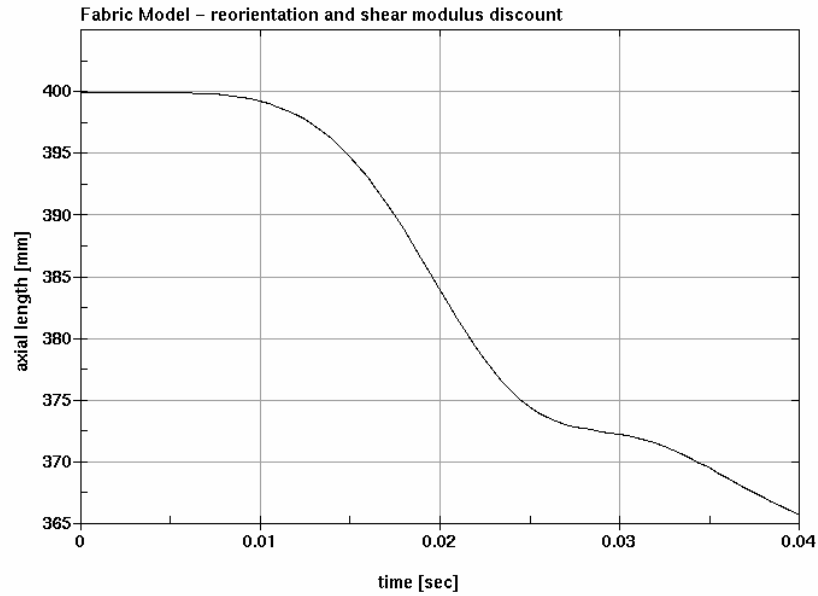
Fig. 3. Axial length change of short airbag with loosely woven fabric model.
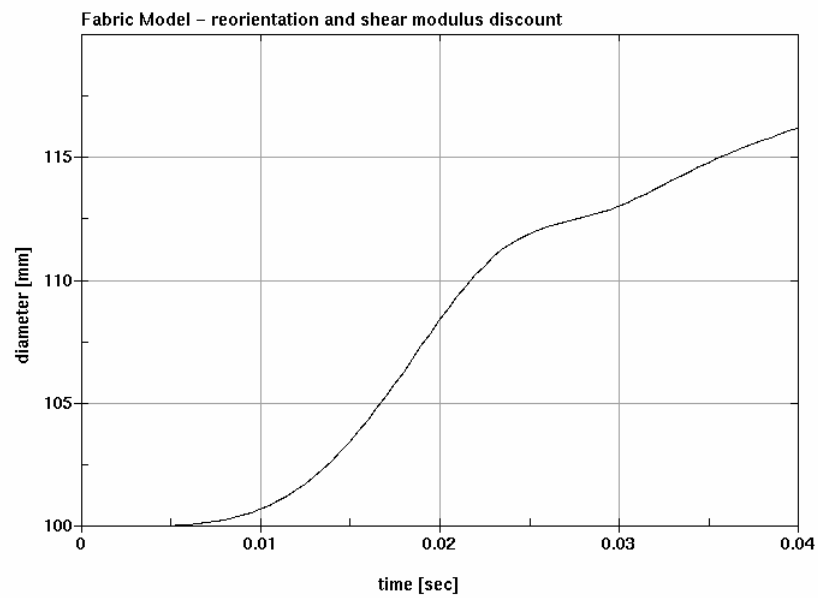
Fig. 4. Diameter change of short airbag with loosely woven fabric model.
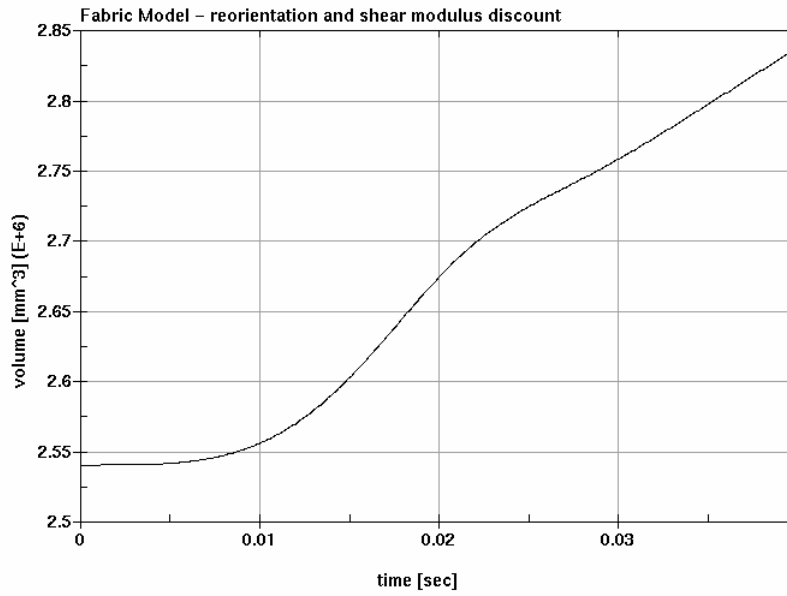
Fig. 5. Volume change of short airbag with loosely woven fabric model.
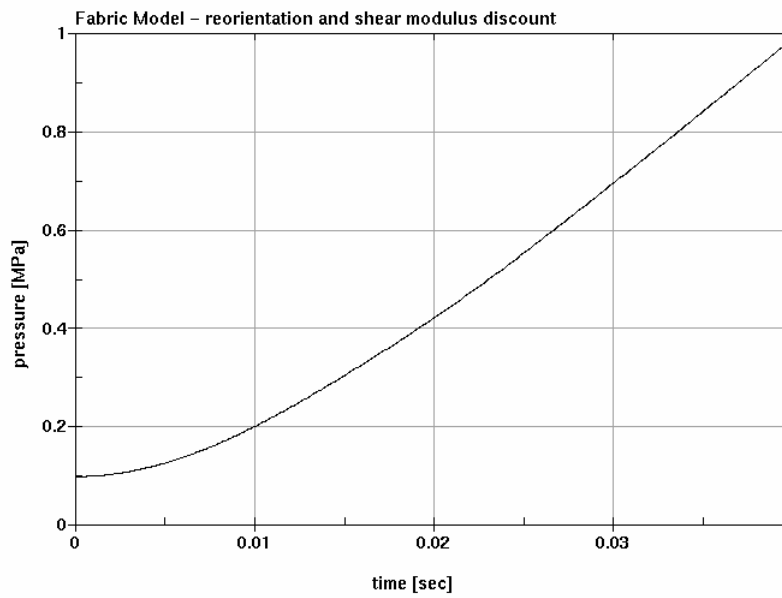
Fig. 6. Pressure change in short airbag with loosely woven fabric model.
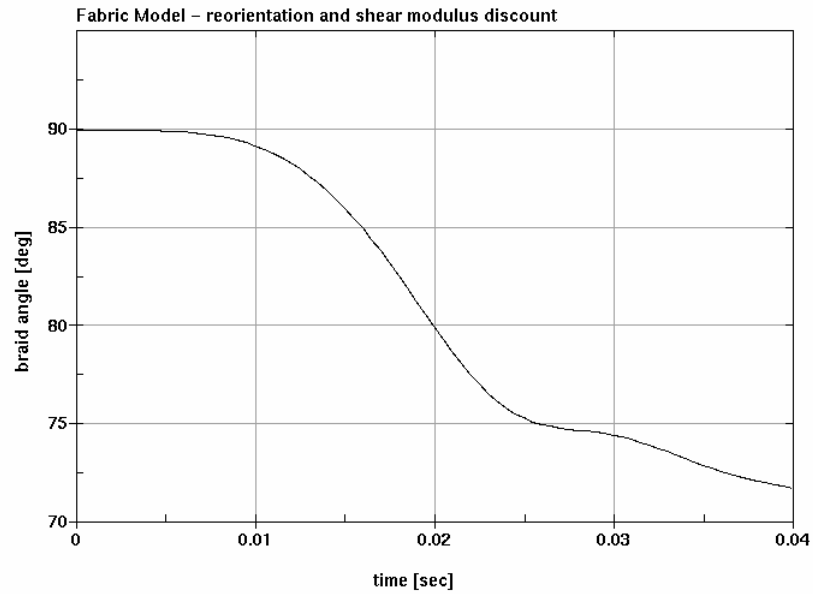
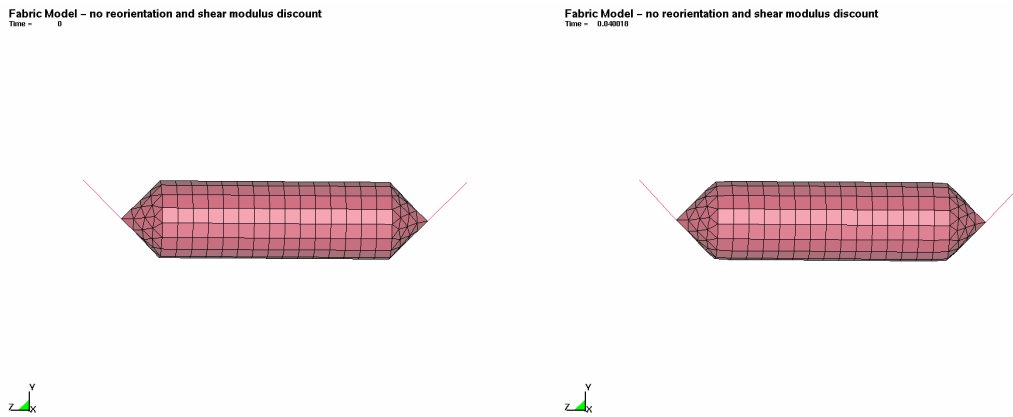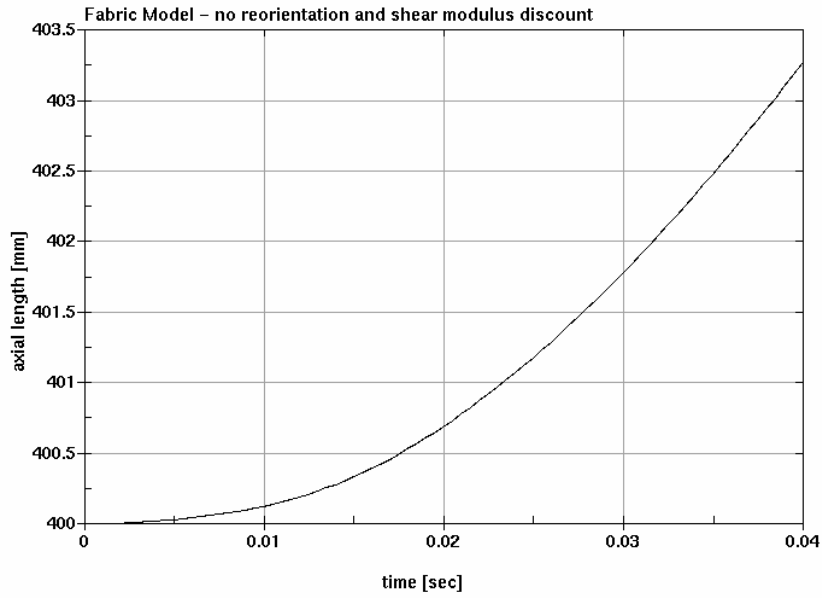Fig. 7. Change of the angle between the yarns for short airbag with loosely woven fabric model.

Fig. 8. Successive states of short airbag with tightened woven fabric model inflation simulation.

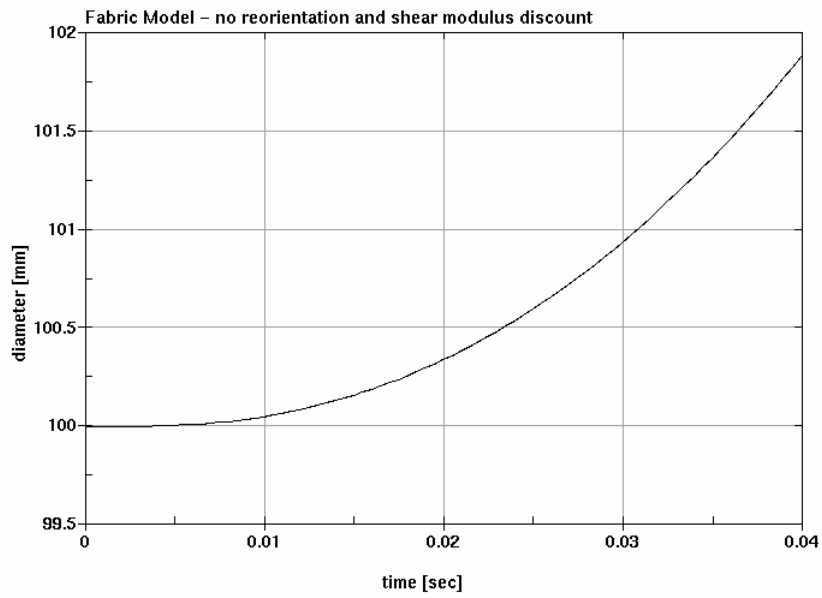Fig. 9. Axial length change of short airbag with tightened woven fabric model.

Fig. 10. Diameter change of short airbag with tightened woven fabric model.
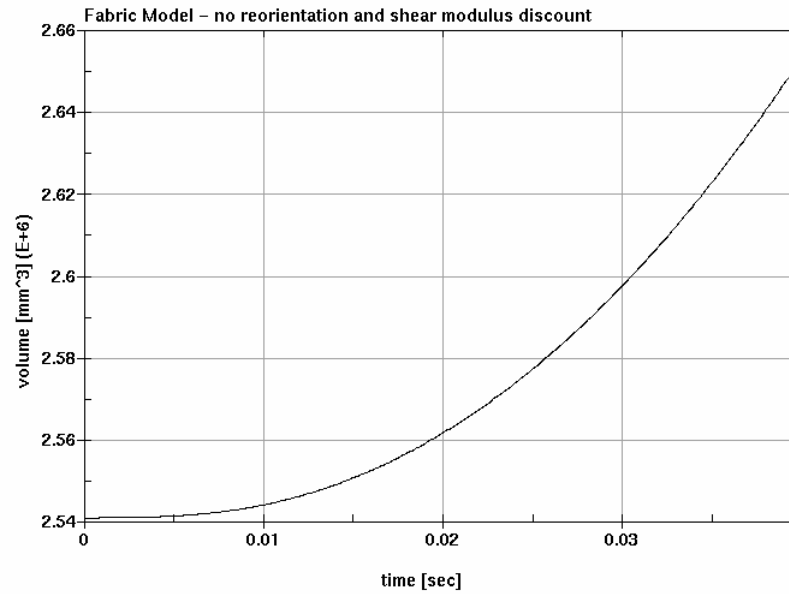
Fig. 11. Volume change of short airbag with tightened woven fabric model.
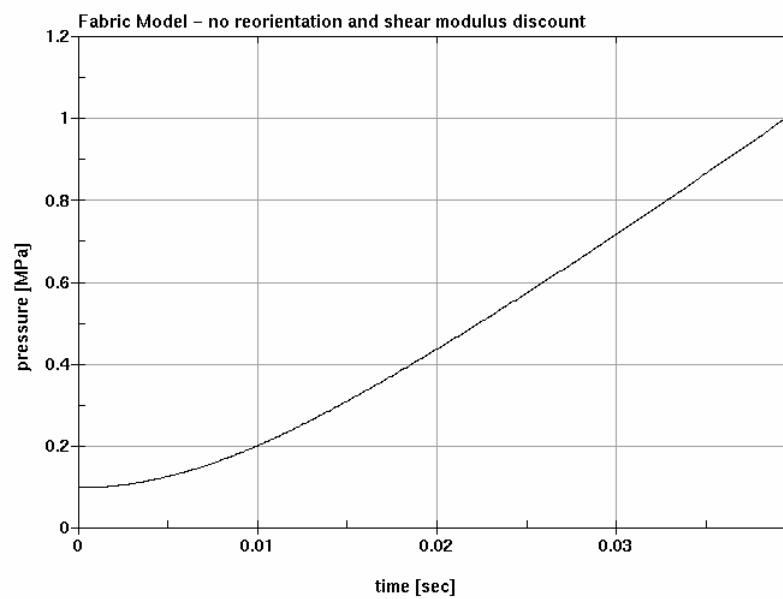

Fig. 12. Pressure change in short airbag with tightened woven fabric model.